

Nanoscale

Accepted Manuscript

This article can be cited before page numbers have been issued, to do this please use: Y. Sun, B. Liu, C. K. Gan, S. Xia, H. Lin, S. Liu and T. Yu, *Nanoscale*, 2025, DOI: 10.1039/D4NR04743E.



This is an Accepted Manuscript, which has been through the Royal Society of Chemistry peer review process and has been accepted for publication.

Accepted Manuscripts are published online shortly after acceptance, before technical editing, formatting and proof reading. Using this free service, authors can make their results available to the community, in citable form, before we publish the edited article. We will replace this Accepted Manuscript with the edited and formatted Advance Article as soon as it is available.

You can find more information about Accepted Manuscripts in the [Information for Authors](#).

Please note that technical editing may introduce minor changes to the text and/or graphics, which may alter content. The journal's standard [Terms & Conditions](#) and the [Ethical guidelines](#) still apply. In no event shall the Royal Society of Chemistry be held responsible for any errors or omissions in this Accepted Manuscript or any consequences arising from the use of any information it contains.

Strong and Reciprocal Magneto-Phonon effects in a 2D Antiferromagnetic Semiconductor FePSe₃

Yue Sun ‡^a, Bo Liu ‡^a, Chee Kwan Gan^b, Shian Xia^a, Haoyun Lin^a, Sheng Liu^{*a},
Ting Yu^{*ac}

*Corresponding authors

^a School of Physics and Technology, Wuhan University, Wuhan 430072, China;

E-mail: liu.sheng@whu.edu.cn and yu.ting@whu.edu.cn

^b Institute of High Performance Computing (IHPC), Agency for Science, Technology and Research (A*STAR), 1 Fusionopolis Way, #16-16 Connexis, Singapore 138632, Republic of Singapore

^c Wuhan Institute of Quantum Technology, Wuhan 430206, China

‡ These authors contributed equally to this work.



Abstract

Magnon-phonon coupling and spin-phonon interaction, both of which are interplays between phonons and magnetism, provide a new way to manipulate phonons. Two-dimensional (2D) magnetic systems are anisotropic in their magnetic order and may have magnons carrying spin angular momentum. According to recent reports, angular momentum can be transferred by the interaction of magnons and phonons. Here focusing on two additional features in the Raman spectra at low frequencies that appear below the Neel temperature, we report that we can control the interplay between spin and lattice vibration and the energy of phonons coupled with magnons by changing the excitation laser power in the 2D antiferromagnetic FePSe₃ which possesses the magnon-phonon coupling with the absence of external magnetic field. On the other hand, at high frequency of Raman spectra, another spin-phonon Raman scattering was observed in FePSe₃. Our results show that out-of-plane magnetic field can control phonons and induce a Raman scattering rotation of A_g mode. In this work, we provide a method of local heating to regulate the phonons coupled with magnons and reveal a spin-phonon phenomenon in antiferromagnetic material.



1. Introduction

The discovery of two-dimensional (2D) magnetic materials such as CrI_3 ¹ and $\text{Cr}_2\text{Ge}_2\text{Te}_6$ ² in 2017 marked a significant milestone in condensed matter physics. These materials exhibit long-range magnetic order even when reduced to a single atomic layer. According to the Mermin-Wagner theorem³, thermal fluctuations in a 2D isotropic Heisenberg model would destroy any long-range magnetic order, preventing spontaneous magnetization. However, the magnetic anisotropy observed in materials like CrI_3 and $\text{Cr}_2\text{Ge}_2\text{Te}_6$ compensates the impact of thermal fluctuations, thus allowing for the stabilization of long-range magnetic order in two dimensions. The emergence of 2D van der Waals (vdWs) magnetic materials and the ability to engineer their unique electronic and magnetic properties⁴⁻⁶ have tuned multiple physical effects, such as giant magnetoresistance (GMR)⁷ and tunnel magnetoresistance (TMR),⁸ enabling the 2D magnetic materials to serve as a promising platform for specific applications in spintronics and magnetic storage.

Magnonics, as a distinct field from spintronics, focusing on the study of high-frequency information propagating and processing with manipulation of spin waves (magnons), has gained significant traction with the advent and rapid development of 2D magnetic materials and spin dynamics.⁹⁻¹² Thus, the study of magnons has been observed in several materials, such as CrI_3 ,^{13,14} MnBi_2Te_4 ¹⁵ and MnPS_3 ¹⁶ and attracted increasing attention, due to the fact that magnons can offer lower energy consumption and have shorter wavelengths than the charge-based devices,^{10,17} which can lead to more compact and miniaturized devices. However, the current generation of magnons faces inefficiency due to its dependence on the conversion of uncontrollable thermal energy.¹⁸⁻²¹

The interplay between spin and lattice further enriches the field of 2D magnonics with the participation of phonons which can propagate long distance in materials, reducing energy dissipation and processing information more efficiently. As a dynamic form of spin-lattice interactions, the magnon-phonon coupling, which provides precise control of magnons, has arisen particular interest.²²⁻²⁵ Moreover, previous research



projects have demonstrated the energy of magnons more coincides with phonons in antiferromagnetic materials (AFM) than ferromagnetic materials (FM), due to AFM exhibit inherent high frequencies (two orders of magnitude higher than ferromagnetic materials).^{26–29} MPX_3 (where $M = Fe, Cr, Co, Mn, Ni$ and $X = S$ or Se),^{30,31} one of the families in typical AFM, has shown great potential in the research of magnon-phonon coupling.^{23,32} A strong magnon-phonon coupling has been directly discovered in $FePS_3$ at high magnetic fields by Raman spectroscopy.³³ Thin $FePSe_3$ makes the magnon and phonon couple at 0T as a reality.³⁴ This allows MPX_3 to be ideal platforms for coupling of magnons and phonons. Effective control and management of phonons and magnons are significant challenges in contemporary physics and materials science. Electric fields, magnetic fields, and strain are commonly employed to regulate phonons. But in many cases, the propagation of magnons and phonons in magnonics devices requires the maintenance of global magnetic order. Local control of magnon-phonon coupling allows for the localized tuning of magnon properties without affecting the overall magnetic order. Consequently, for thin 2D vdWs materials, laser-induced local thermal modulation may be an effective approach for their device applications.³⁵ However, phonons exhibit low sensitivity to temperature, making it difficult to achieve precise control through temperature manipulation. Moreover, phonons related to magnetic order are more susceptible to the influence of magnetic fields than phonons that are unrelated to magnetism. So far, another interaction between spins and phonons which can manipulate pure phonons under magnetic field with the absence of magnons and induce Raman scattering rotation has also been observed in 2D non-magnetic MoS_2 ,³⁶ $InSe$ ³⁷ and magnetic material $CrBr_3$.³⁸ Furthermore, the nonreciprocal change of polarized Raman intensity also was found in magnetic material CrI_3 .³⁹ These research findings provide new insights and application directions for the fundamental properties of phonons and their role in magnetic materials. However, how this spin-phonon interaction behaves in AFM is still unclear.

In this article, we report the spatially localized control of spin fluctuation by local laser heating to modulate magnon-phonon coupling and the energy of phonons coupled



with magnons in the irradiated region without altering the global magnetic order, combined with Raman spectroscopy of 2D AFM FePSe₃. Our result also unambiguously demonstrates the existence of two degenerate phonon modes in this material by laser heating at 0T and 6T, these two phonons have opposite angular momentum and selectively interact with the spin-up and spin-down magnons. Besides, we observed spin-phonon interaction which induces the giant reciprocal rotation in FePSe₃ of A_g mode at high frequency of Raman spectra. The intensities of XX and XY polarization configuration show significantly change when the out of plane magnetic field is applied. The direction of polarization rotates counterclockwise (clockwise) when a positive (negative) magnetic field is applied, while the direction of polarization changes clockwise when a negative magnetic field is applied.

2. Results and discussion

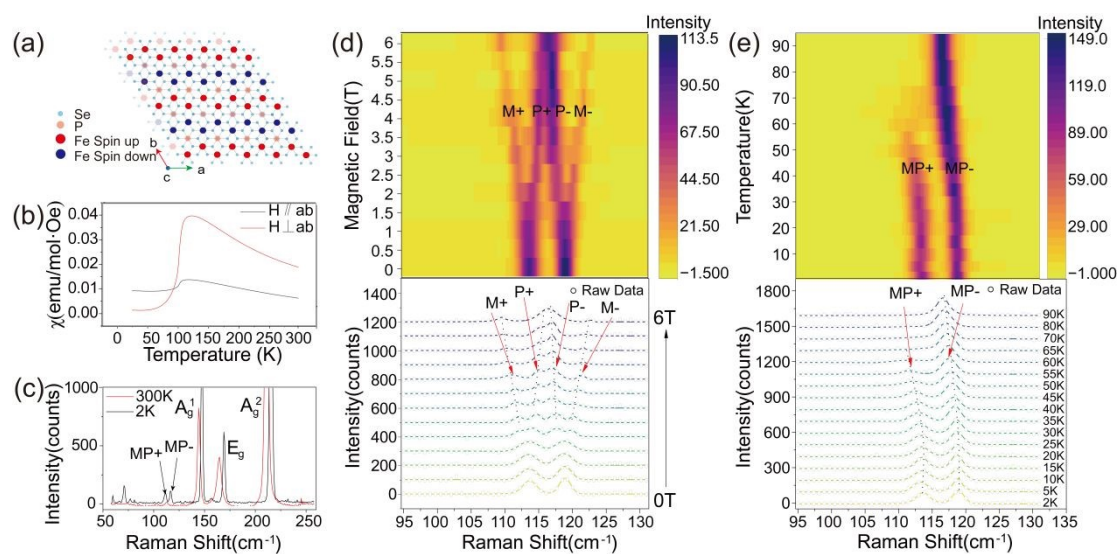


Fig. 1 (a) Top-view of the FePSe₃ crystal structure and its magnetic ordering. (b) The magnetic susceptibility of FePSe₃. (c) Comparative Raman spectra of few-layer FePSe₃ at 300 K and 2 K. MP indicates the magnon-phonon coupled mode, where MP+ (MP-) refers to the coupling between spin-up (spin-down) magnons and phonons (d) Raman intensity mapping and corresponding spectra of FePSe₃ at 2 K as a function of the magnetic field. M denotes the magnon peak, with M+ (M-) representing spin-up (spin-down) magnons. The two degenerate phonon modes, labeled as P, undergo splitting under magnon interactions. The resulting non-degenerate phonons coupled to



spin-up (spin-down) magnons are denoted as P+ (P-) (e) Temperature dependence of low-energy magnon-phonon (MP) branches Raman modes in few-layer FePSe₃, measured from 2 K to 90 K at zero magnetic field.

Transition metal phosphorus trichalcogenides (MPX₃, where M = Fe, Mn, Ni, and X = S, Se) are a family of van der Waals antiferromagnetic semiconductors,^{30,31} whose monolayer counterparts present intralayer antiferromagnetism. Among them, FePSe₃ is promising for spintronics and magnonics, due to its combination of antiferromagnetism and narrower band gap (~1.3 eV). Its crystal structure belongs to the trigonal R $\bar{3}$ space group and the top view is illustrated in Fig. 1a. At its magnetic ground state, the Fe atoms in a monolayer FePSe₃ lattice form a 2D hexagonal spin lattice, containing a zigzag antiferromagnetic (AFM) order.⁴⁰ The magnetic moments at Fe sites alternate between spin-up and spin-down configurations along the Z-axis on adjacent chains. As corroborated by temperature-dependent magnetic susceptibility curve presented in Fig. 1b, the change of perpendicular ($H \perp ab$) magnetic susceptibility is much larger than that of parallel ($H // ab$), pointing to a signature of strong magnetic anisotropy of the whole system in FePSe₃ that is consistent with its well-known Ising type magnetic order, which is out of plane.

Fig. 1c exhibits the Raman spectra of a few-layer FePSe₃ flake (about 25 nm, as shown in Fig. S1) on 280 nm SiO₂/Si substrate at 300 K and 2 K, respectively. The main Raman modes at higher frequencies ($> 120 \text{ cm}^{-1}$) primarily arise from the vibrations of the [P₂Se₆]⁴⁻ units, and thus indicate blueshift with decreasing temperature. The Raman features emerging at lower frequency (~75 cm⁻¹ and 117 cm⁻¹) have been attributed to the vibrations of Fe²⁺ ions which turn into Raman-active modes after the phase transition from paramagnetic to AFM states.^{41,42} Interestingly, the Raman mode at 117 cm⁻¹ “splits” into two modes upon the AFM transition. Some recent works claimed that these two additional features in Fig. 1c are the magnon-phonon coupling modes which are designated as MP, with MP+ (MP-) specifically indicating the coupling between phonon and spin-up (spin-down) magnon. By increasing external magnetic fields along



the out-of-plane direction, the two MP modes split to four peaks (M⁺, P⁺, P⁻ and M⁻), as shown in Fig. 1d. The M⁺ (blue up triangles) and M⁻ (purple down triangles) show Zeeman splitting at higher magnetic fields (> 1.5 T) with a *g*-factor of -0.71 and 0.66 cm⁻¹/T, respectively (shown in Fig. S2), verifying their magnon essence. Meanwhile, the P⁺ and P⁻ depart from M⁺ and M⁻, respectively, and merge into one peak whose peak position is no longer dependent on the fields. Fig. 1d presents the temperature-dependent Raman spectra of FePSe₃ at 0 T. At low temperature range (<30 K), MP⁺ and MP⁻ show negligible temperature dependence. As the temperature exceeds 30 K, dramatical red shift takes place for both two peaks. At high temperature range (>60 K), MP⁺ mode disappears completely while “MP⁻” restore to temperature independent.

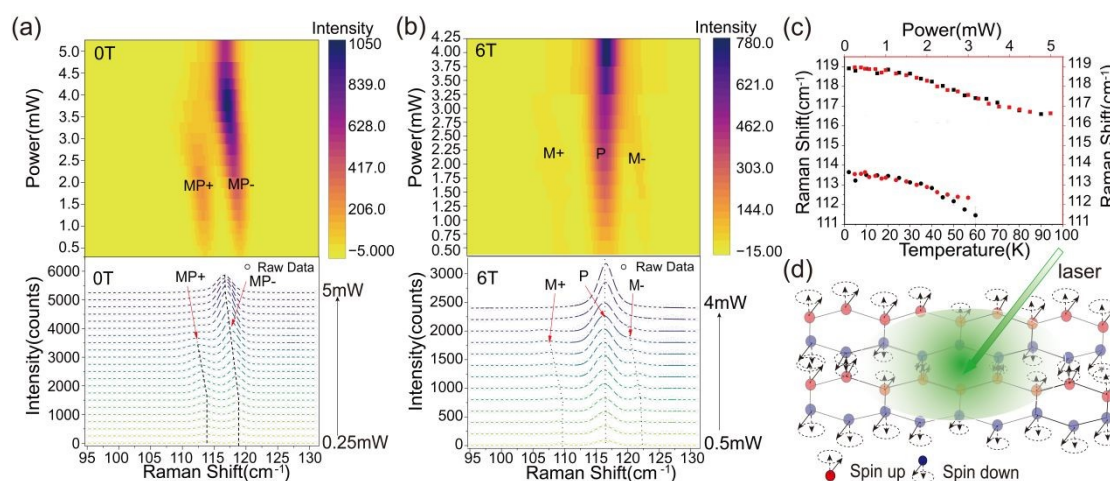


Fig. 2 (a), (b) The laser power dependence Raman spectrum of low-energy magnon-phonon (MP) branches in few-layer FePSe₃ at 0T and 6T, respectively. (c) The peak position of Raman as a function of laser power and temperature at 0T. Circles denote MP⁺ and squares denote MP⁻, with black indicating temperature-dependent parameters and red representing power-dependent parameters. (d) Schematic diagram of local tuning of magnon properties by laser heating.

In FePSe₃, the phonon vibrational frequency and magnon procession frequency are coincidentally in resonance, in stark contrast to FePS₃ where the magnon needs high magnetic fields driven Zeeman shift to reach resonance energy with the adjacent phonon. They could be very close or even overlay if strong coupling between the two



quasiparticles does not exist. The temperature- and field-dependent evolutions of MP+ and MP- both verify the existence of strongly coupled magnon-phonon at zero field. The increase in temperature globally changes the magnetic fluctuations, magnon and phonon populations, leading to the energy shift and change of coupling strength. To modify and detect the strong coupling locally, we performed power-dependent Raman scattering measurements on a few-layer FePSe₃ flake.

The evolution of the Raman spectra with varying laser power from 0.25mW to 5mW at 0T, is depicted in Fig. 2a. At mild laser powers (e.g., <1mW), the MP+ and MP- branches (energy and peak intensity) are negligibly modified. As the laser power exceeds 1mW, the peak positions of MP+ and MP- begin to exhibit an obvious redshift, from 113.8 and 118.9 cm⁻¹ to 111.4 and 116.9 cm⁻¹, respectively. At higher laser power (> 3mW), the MP+ branch vanishes as its signal intensity significantly decreases, while the MP- branch “merges” into the phonon mode labeled as “P”. The energy redshift of MP- saturates when laser power up to ~4.5 mW. Interestingly, the laser-power-dependence (Fig. 2a) and the temperature-dependence (Fig. 1e) of the Raman spectral energy position match very well at 0 T, implying that the sample is locally heated by the laser power. In this manner, the power-dependent Raman spectra of FePSe₃ at 6 T (Fig. 2b) experiences similar temperature modification. The dotted lines in Fig. 2a and Fig. 1e represent the red-shift of the Raman peaks, which are plotted versus laser power (red traces and axis) and temperature (black traces and axis) in Fig. 2c. By mirroring the two sets of traces, the temperature of the laser spot is accurately evaluated.

In general, phonons and magnons are subject to Bose-Einstein statistics but operate in different energy regimes. The energy required to excite phonons is typically higher than that for magnons, making phonons less sensitive to temperature. As laser power increases, the high-wavenumber Raman peaks of FePSe₃ (as shown in Fig. S3) remain unchanged, while the low-wavenumber MP+ and MP- peaks redshift predominantly. Since MP+ and MP- contain strongly coupled magnons and phonons, their sensitivity to temperature can be attributed to the contribution from either the low-wavenumber phonons or the magnons. According to the field-dependent Raman spectra



(Fig. 1d), the magnons and phonons are completely decoupled at high magnetic fields (e.g., 6 T). Therefore, at 6 T, by increasing the laser power, the magnons and phonons are modified separately which fit well with temperature-dependent Raman spectra (Fig. S4b). At this point, the magnons (M^+ and M^- branches) exhibit a redshift, while the phonon (P) barely changes in frequency (Fig. S4a). This indicates that the low-wavenumber phonon is nearly independent of temperature and the redshift of MP^+ and MP^- mainly originate from the frequency change of magnons. It also unambiguously proves that the strong coupling at 0 T arises from a pair of degenerate phonons and two branches of antiferromagnetic magnons. Circular polarized Raman in Figure S8 shows the chirality of the two branches. The left- and right-handed chirality of lattice vibration selectively interact with the spin-up and spin-down magnons, topologically protecting the strong coupling.^[34] In addition, the laser power can locally decouple the magnon and phonon, thus adding an important controlling knob to the potential magnonic devices based on FePSe_3 , and it is the interaction between magnons and phonons that modulates the phonon energy under local heating.

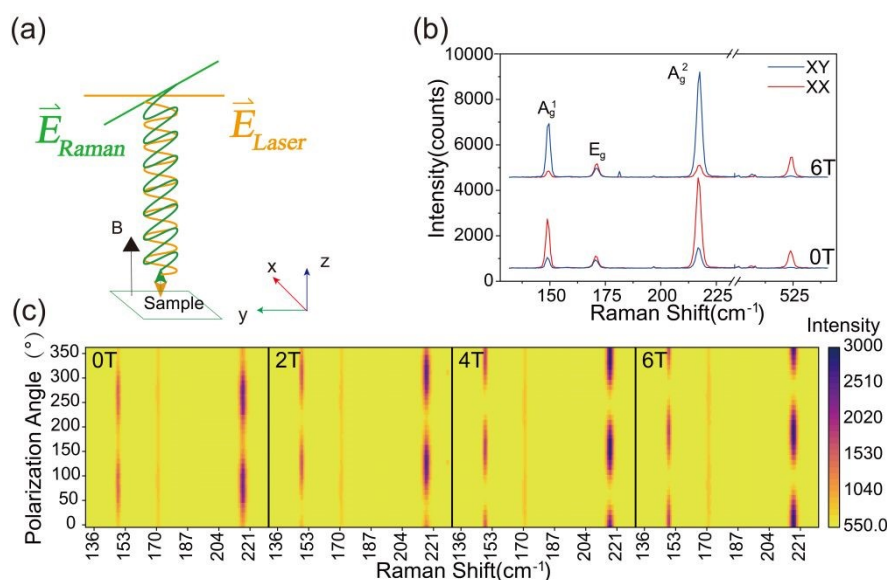


Fig. 3 (a) experiment diagram of polarization Raman scattering. The polarization of incident laser is along the y-axis while the scattering laser has an angle with y axis with the magnetic field. (b) The parallel and perpendicular polarization A_g^1 , E_g and A_g^2 Raman mode of FePSe_3 and Si with the magnetic field at 0T and 6T. (c) The 2D maps of linear polarization Raman spectra of FePSe_3 with



the magnetic field at 0T, 2T, 4T, 6T, respectively.

View Article Online
DOI: 10.1039/D4NR04743E

Besides the magnon-phonon strong coupling at low frequencies, the magneto-Raman effects of the high frequency phonons also show prominent field-dependence. The Raman spectrum of phonons at 149.6cm^{-1} and 217.5cm^{-1} with A_g symmetry exhibit an apparent anisotropic polarization dependence behavior and display a marked twofold rotational symmetry. In contrast, the phonon at 171.5cm^{-1} with E_g symmetry is not sensitive to the polarization configuration, indicating that the in-plane E_g vibration mode is isotropic (Fig. S4). Fig. 3a shows the experiment diagram of polarization Raman spectroscopy. The linear polarized incident light is directed vertically to the surface of the sample FePSe_3 and the Raman scattering is also normal to the surface, with the magnetic field applied along the z-axis. Fig. 3b shows the Raman spectrum of the Raman scattering parallel to the incident light (XX) and perpendicular to the incident light (XY), under the out-of-plane magnetic field at 0T and 6T, respectively. The relative Raman intensities of the XX and XY polarization configurations measured for the A_g modes change significantly with the magnitude of the applied magnetic field, while the intensity of E_g mode remains unchanged and is found to be independent of the magnetic field. In contrast to FePSe_3 , the scattering polarization of silicon also shows no dependence on the magnetic field, although a twofold anisotropic pattern is also observed, as shown in Fig. S5 and S6. Therefore, this indicates that the observed phenomenon specifically occurs in the out-of-plane A_g mode phonons in 2D AFM FePSe_3 in the presence of the magnetic field. To further elucidate the effect of the magnetic field on the polarization Raman intensity of the A_g modes, angle-dependent maps of linear polarization Raman scattering of FePSe_3 are presented in Fig. 3c, with the magnetic field varying from 0T to 6T. The results show that the polarization direction of the two A_g modes rotates significantly with increasing magnetic field strength, while the intensity of the E_g mode remains constant. Additionally, the polarization axes of the A_g^1 and A_g^2 modes exhibit identical directions and angles of rotation under the same magnetic field. This spin-phonon optical phenomenon has



previously been reported in the non-magnetic 2D material MoS₂.⁴³ As illustrated schematically in Fig. 3a, under an out-of-plane magnetic field, there is an angular deviation between the Raman scattering and the incident light. This phenomenon can be attributed to the Lorentz force acting on the local *d*-orbital electrons involved in the Raman scattering process, induced by the external magnetic field.

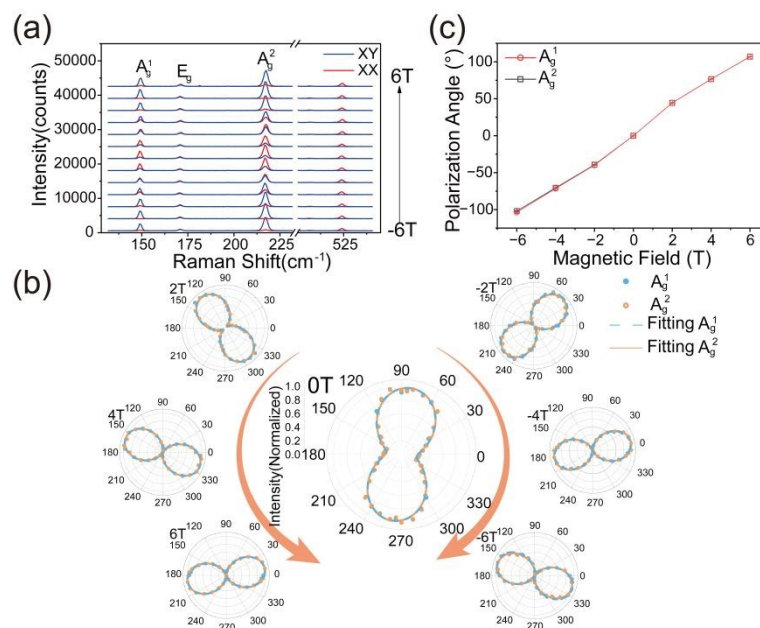


Fig. 4 (a) The parallel and perpendicular polarization Raman of FePSe₃ and Si with magnetic field from -6T to 6T. (b) The linear polarization Raman of FePSe₃ with magnetic field from -6T to 6T. (c) The rotation angle of polar Raman.

To further verify this phenomenon, we measured the Raman scattering under the opposite magnetic field. The XX and XY polarization configurations of the Raman spectrum with the magnetic field from -6 T to 6 T is shown in Fig. 4a. The A_g modes intensity of XX polarization decreases with the magnetic field increasing from 0T to 5T and reaches the minimum at 5T, then increasing with the field over 5T, while XY configurations exhibit antiparallel behavior. Meanwhile, the negative magnetic field exhibits the same tendency. Additionally, the Raman scattering intensity of the A_g¹ and A_g² modes as a function of polarization angle under magnetic fields from -6T to 6T has also been measured, as shown in Fig. 4c. The polarization axis is parallel to the direction



of the incident polarized light at 0T. The rotation direction of the polarization axis reverses when the direction of the magnetic field is reversed. When a positive magnetic field is applied, the direction of polarization rotates counterclockwise, while the direction of polarization changes clockwise when the negative magnetic field is applied. More obviously, the rotation angle is remarkably giant, as shown in Fig. 4b and 4c. The polarization axis is rotated from -107° to 102° as the magnetic field varies from -6T to $+6\text{T}$ and the absolute values of polarization rotation angles are equal in the positive and negative magnetic field, shown in Fig. 4b, which is different from the magnetic material CrI_3 .³⁸ The frequency, line width, and peak shape of Raman do not change, indicating that the magnetic field has no effect on the lattice structure.

This phenomenon can be explained by the fact that when the FePSe_3 transfers from non-magnetic to antiferromagnetic case, the time-reversal symmetry is broken, which can induce an antisymmetric component in the Raman tensors.

When there is no magnetic field applied, the Raman tensor of FePSe_3 in antiferromagnetic state is

$$\begin{pmatrix} a & i\beta & 0 \\ -i\beta & a & 0 \\ 0 & 0 & b \end{pmatrix}$$

When the magnetic field is applied normal to the sample surface, the Lorentz force will induce the motion of electron in plane, and this changes the electronic susceptibility $\alpha(B)$ and modifies the Raman tensor elements. The magnetic field dependence $\alpha(B)$ can be derived by considering the Lorentz force. In a 2D case, the kinetic equations for electrons driven by a magnetic field can be written as

$$\begin{cases} \ddot{x} + \gamma\dot{x} + \omega_0^2 x = -\frac{eE}{m} e^{i\omega t} - \frac{eB}{m} \dot{y} \\ \ddot{y} + \gamma\dot{y} + \omega_0^2 y = -\frac{eB}{m} \dot{x} \end{cases}$$

Thus the

$$\begin{cases} x = \frac{iE}{\omega} \frac{B_0}{B_0^2 + B^2} \\ y = \frac{iE}{\omega} \frac{B}{B_0^2 + B^2} \end{cases}$$

Then we can get the electronic susceptibility



$$\begin{cases} a_{xx}(B) = a_{yy}(B) = -\frac{ex}{E} \propto \frac{B_0}{B_0^2 + B^2} \\ a_{xy}(B) = a_{yx}(B) = -\frac{ey}{E} \propto \frac{B}{B_0^2 + B^2} \end{cases}$$

Where $B_0 = \frac{m\gamma}{e} \left[1 - i \frac{(\omega_0^2 - \omega^2)}{\gamma\omega} \right]$, When the applied magnetic field is close to the value B_0 , it has the greatest effect on the Raman intensity. So the Raman tensor of A_g now can be written as

$$A_g = \begin{pmatrix} a \cdot a_{xx}(B) & i\beta \cdot a_{yx}(B) & 0 \\ -i\beta \cdot a_{xy}(B) & a \cdot a_{yy}(B) & 0 \\ 0 & 0 & b \end{pmatrix}$$

The intensity of Raman scattering is given by

$$I \propto |e_s \cdot R \cdot e_i|^2 = \left| (1 \ 0 \ 0) \cdot \begin{pmatrix} a \cdot a_{xx}(B) & i\beta \cdot a_{yx}(B) & 0 \\ -i\beta \cdot a_{xy}(B) & a \cdot a_{yy}(B) & 0 \\ 0 & 0 & b \end{pmatrix} \begin{pmatrix} \cos(\theta) \\ \sin(\theta) \\ 0 \end{pmatrix} \right|^2$$

Therefore the $I_{xx} \propto \left| \frac{aB_0}{B_0^2 + B^2} \right|^2$, $I_{yy} \propto \left| \frac{\beta B}{B_0^2 + B^2} \right|^2$, so the intensity of XX and XY influenced by the magnetic field, and resulting in a transfer of Raman intensity between the two orthogonal polarization configurations. As for the reciprocal phenomenon, compared with ferromagnetic materials, the magnetic moments of antiferromagnetic materials are equal under positive and negative magnetic fields, resulting in the Lorentz force being consistent under positive and negative magnetic fields.

This newly observed phenomena exhibit signals several times stronger than traditional magneto-optical effects, such as the Kerr and Faraday effects, providing a new method for magneto-optical characterization. Moreover, using magnetic field instead of other external field to control the polarization of Raman modes is of great significance, as it offers a new way to manipulate phonons that are unrelated to magnetism. This control not only deepens the understanding of interactions between spins, phonons, and photons but also significantly expands the application scope and design freedom of magnonic devices, playing a very important role in the application of magnonics.

3. Conclusions



In summary, we unambiguously prove the magnon-phonon strong coupling in FePSe₃ at 0 T by combining the field- and power-dependent Raman spectroscopy. The laser power can locally excite the spin fluctuation (the amplitude of spin precession), the population and energy of the AFM magnon are consequently changed, thus modulating the magnon-phonon coupling and phonon energy, thereby adding an important controlling knob to the potential magnonic devices based on FePSe₃. A giant reciprocal spin-phonon interaction was observed. Through time symmetry breaking and Lorentz force on the local *d*-orbital electrons, the polarization axis of the A_g Raman modes can be dramatically rotated by external out-of-plane magnetic field perpendicular to the basal plane. In contrast to the 2D ferromagnetic materials, the rotation of Raman tensor in FePSe₃ is reciprocal and symmetric to positive and negative fields, which is due to the equal magnetic. Our result demonstrates the 2D antiferromagnet FePSe₃ as a unique platform for spintronics and magnons both at zero and high fields.



4. Methods

4.1 Sample preparation

FePSe₃ single crystal was grown using chemical vapor transport reactions (CVT) in vacuum-sealed quartz tube with I₂ as the transport agent. Fe, P and Se powders were loaded in one side of the sealed tube with accurate stoichiometric proportions. The tube was then placed in a tube furnace, aligned to the middle of two heating zones. In two weeks, the source and empty ends of the tube were set at 750 and 650°C, the temperature gradient driving the transport and reaction of chemical vapors, making nucleation and crystal growth happen at the low temperature end. After growth, millimeter sized crystals with flake appearance were obtained. Few-layer FePSe₃ flakes were obtained from FePSe₃ crystal synthesized by CVT via mechanical exfoliation by using polydimethylsiloxane (PDMS), and transferred onto the Si substrates with a layer of 280nm SiO₂. All the measurements were performed at helium environment and low temperature and the sample is very stable.

4.2 Magneto-Raman measurement

The Raman measurements were recorded using a Witec Alpha 300R confocal Raman microscope, based on a closed-cycle helium cryostat (attoDRY2100, attocube) with base temperatures down to 1.8 K and a superconducting magnet (the maximum out of plane magnetic field is up to ± 9 T and in plane is ± 3 T). The 532nm linear polarized laser with was focused perpendicular to the surface of the sample through a 69.94x objective lens (numerical aperture = 0.82) for the Raman measurement at low temperature and magnetic field. The maximum power is kept below than 5 mW to avoid damage to the sample. The Raman signals were first collected by a photonic crystal fiber and then coupled into the spectrometer with 1800 g/mm grating. The polarization-resolved Raman spectra were obtained by rotating the polarization of the analyzer, which was placed before the photonic crystal fiber.

Author Contributions



Y.S. and B.L. contributed equally to this work. Y.S., B.L., S.L., and T.Y. conceived the project and designed the experiments. Y.S., B.L., S.A.X., and H.Y.L. prepared the samples and conducted the experimental measurements. C.K.G. performed the theoretical calculations. Y.S. and B.L. analyzed the data and wrote the manuscript with input from all coauthors. S.L. and T.Y. supervised the whole project.

View Article Online
DOI: 10.1039/D4NR04743E

Data availability

The data that support the findings of this study are available from the corresponding author upon request.

Conflicts of interest

There are no conflicts to declare.

Acknowledgements

This project was supported by the National Key Research and Development Program of China (No. 2021YFA 1200800) and the Start-up Funds of Wuhan University.



Reference

- 1 B. Huang, G. Clark, E. Navarro-Moratalla, D. R. Klein, R. Cheng, K. L. Seyler, D. Zhong, E. Schmidgall, M. A. McGuire, D. H. Cobden, W. Yao, D. Xiao, P. Jarillo-Herrero and X. Xu, *Nature*, 2017, **546**, 270–273.
- 2 C. Gong, L. Li, Z. Li, H. Ji, A. Stern, Y. Xia, T. Cao, W. Bao, C. Wang, Y. Wang, Z. Q. Qiu, R. J. Cava, S. G. Louie, J. Xia and X. Zhang, *Nature*, 2017, **546**, 265–269.
- 3 N. D. Mermin and H. Wagner, *Phys. Rev. Lett.*, 1966, **17**, 1133–1136.
- 4 X. Cheng, Z. Cheng, C. Wang, M. Li, P. Gu, S. Yang, Y. Li, K. Watanabe, T. Taniguchi, W. Ji and L. Dai, *Nat Commun*, 2021, **12**, 6874.
- 5 Y. Deng, Y. Yu, Y. Song, J. Zhang, N. Z. Wang, Z. Sun, Y. Yi, Y. Z. Wu, S. Wu, J. Zhu, J. Wang, X. H. Chen and Y. Zhang, *Nature*, 2018, **563**, 94–99.
- 6 Z. Fei, B. Huang, P. Malinowski, W. Wang, T. Song, J. Sanchez, W. Yao, D. Xiao, X. Zhu, A. F. May, W. Wu, D. H. Cobden, J.-H. Chu and X. Xu, *Nature Materials*, 2018, **17**, 778–782.
- 7 Y. Tian and S. Yan, *Sci. China Phys. Mech. Astron.*, 2013, **56**, 2–14.
- 8 Z. Wang, I. Gutiérrez-Lezama, N. Ubrig, M. Kroner, M. Gibertini, T. Taniguchi, K. Watanabe, A. Imamoğlu, E. Giannini and A. F. Morpurgo, *Nat Commun*, 2018, **9**, 2516.
- 9 A. Barman, G. Gubbiotti, S. Ladak, A. O. Adeyeye, M. Krawczyk, J. Gräfe, C. Adelman, S. Cotofana, A. Naeemi, V. I. Vasyuchka, B. Hillebrands, S. A. Nikitov, H. Yu, D. Grundler, A. V. Sadovnikov, A. A. Grachev, S. E. Sheshukova, J.-Y. Duquesne, M. Marangolo, G. Csaba, W. Porod, V. E. Demidov, S. Urazhdin, S. O. Demokritov, E. Albisetti, D. Petti, R. Bertacco, H. Schultheiss, V. V. Kruglyak, V. D. Poimanov, S. Sahoo, J. Sinha, H. Yang, M. Münzenberg, T. Moriyama, S. Mizukami, P. Landeros, R. A. Gallardo, G. Carlotti, J.-V. Kim, R. L. Stamps, R. E. Camley, B. Rana, Y. Otani, W. Yu, T. Yu, G. E. W. Bauer, C. Back, G. S. Uhrig, O. V. Dobrovolskiy, B. Budinska, H. Qin, S. Van Dijken, A. V. Chumak, A. Khitun, D. E. Nikonov, I. A. Young, B. W. Zingsem and M. Winklhofer, *J. Phys.: Condens. Matter*, 2021, **33**, 413001.
- 10 S. Neusser and D. Grundler, *Advanced Materials*, 2009, **21**, 2927–2932.
- 11 P. Pirro, V. I. Vasyuchka, A. A. Serga and B. Hillebrands, *Nature Reviews Materials*, 2021, **6**, 1114–1135.
- 12 B. Flebus, D. Grundler, B. Rana, Y. Otani, I. Barsukov, A. Barman, G. Gubbiotti, P. Landeros, J. Akerman, U. Ebels, P. Pirro, V. E. Demidov, K. Schultheiss, G. Csaba, Q. Wang, F. Ciubotaru, D. E. Nikonov, P. Che, R. Hertel, T. Ono, D. Afanasiev, J. Mentink, T. Rasing, B. Hillebrands, S. V. Kusminskiy, W. Zhang, C. R. Du, A. Finco, T. Van Der Sar, Y. K. Luo, Y. Shiota, J. Sklenar, T. Yu and J. Rao, *J. Phys.: Condens. Matter*, 2024, **36**, 363501.
- 13 J. Cenker, B. Huang, N. Suri, P. Thijssen, A. Miller, T. Song, T. Taniguchi, K. Watanabe, M. A. McGuire, D. Xiao and X. Xu, *Nature Physics*, 2021, **17**, 20–25.
- 14 A. McCreary, T. T. Mai, F. G. Utermohlen, J. R. Simpson, K. F. Garrity, X. Feng, D. Shcherbakov, Y. Zhu, J. Hu, D. Weber, K. Watanabe, T. Taniguchi, J. E. Goldberger, Z. Mao, C. N. Lau, Y. Lu, N. Trivedi, R. Valdés Aguilar and A. R. Hight Walker, *Nat Commun*, 2020, **11**, 3879.
- 15 D. Lujan, J. Choe, M. Rodriguez-Vega, Z. Ye, A. Leonardo, T. N. Nunley, L.-J. Chang, S.-F. Lee, J. Yan, G. A. Fiete, R. He and X. Li, *Nature Communications*, 2022, **13**, 2527.
- 16 W. Xing, L. Qiu, X. Wang, Y. Yao, Y. Ma, R. Cai, S. Jia, X. C. Xie and W. Han, *Phys. Rev. X*, 2019, **9**, 011026.
- 17 A. V. Chumak, V. I. Vasyuchka, A. A. Serga and B. Hillebrands, *Nature Phys*, 2015, **11**, 453–461.
- 18 Y. Wang, D. Zhu, Y. Yang, K. Lee, R. Mishra, G. Go, S.-H. Oh, D.-H. Kim, K. Cai, E. Liu, S. D. Pollard, S. Shi, J. Lee, K. L. Teo, Y. Wu, K.-J. Lee and H. Yang, *Science*, 2019, **366**, 1125–1128.
- 19 J. Han, P. Zhang, J. T. Hou, S. A. Siddiqui and L. Liu, *Science*, 2019, **366**, 1121–1125.



- 20 W. Xing, L. Qiu, X. Wang, Y. Yao, Y. Ma, R. Cai, S. Jia, X. C. Xie and W. Han, *Phys. Rev. X*, 2019, **9**, 011026. [View Article Online](#)
DOI: 10.1039/D4NR04743E
- 21 H. Fulara, M. Zahedinejad, R. Khymyn, A. A. Awad, S. Muralidhar, M. Dvornik and J. Åkerman, *Sci. Adv.*, 2019, **5**, eaax8467.
- 22 D. A. Bozhko, V. I. Vasyuchka, A. V. Chumak and A. A. Serga, *Low Temperature Physics*, 2020, **46**, 383–399.
- 23 T. T. Mai, K. F. Garrity, A. McCreary, J. Argo, J. R. Simpson, V. Doan-Nguyen, R. V. Aguilar and A. R. H. Walker, *Sci. Adv.*, 2021, **7**, eabj3106.
- 24 K. Wang, J. He, M. Zhang, H. Wang and G. Zhang, *Nanotechnology*, 2020, **31**, 435705.
- 25 D. Lanifmmode \mbox{\else \fion, H. C. Walker, E. Ressouche, B. Ouladdiaf, K. C. Rule, G. J. McIntyre, T. J. Hicks, H. M. Rønnow and A. R. Wildes, *Phys. Rev. B*, 2016, **94**, 214407.
- 26 T. Jungwirth, X. Marti, P. Wadley and J. Wunderlich, *Nature Nanotech.*, 2016, **11**, 231–241.
- 27 S. M. Rezende, A. Azevedo and R. L. Rodríguez-Suárez, *Journal of Applied Physics*, 2019, **126**, 151101.
- 28 J. R. Hortensius, D. Afanasiev, M. Matthiesen, R. Leenders, R. Citro, A. V. Kimel, R. V. Mikhaylovskiy, B. A. Ivanov and A. D. Caviglia, *Nat. Phys.*, 2021, **17**, 1001–1006.
- 29 M. A. Weiss, A. Herbst, J. Schlegel, T. Dannegger, M. Evers, A. Donges, M. Nakajima, A. Leitenstorfer, S. T. B. Goennenwein, U. Nowak and T. Kurihara, *Nat Commun.*, 2023, **14**, 7651.
- 30 K. Du, X. Wang, Y. Liu, P. Hu, M. I. B. Utama, C. K. Gan, Q. Xiong and C. Kloc, *ACS Nano*, 2016, **10**, 1738–1743.
- 31 R. Samal, G. Sanyal, B. Chakraborty and C. S. Rout, *J. Mater. Chem. A*, 2021, **9**, 2560–2591.
- 32 D. J. Gillard, D. Wolverson, O. M. Hutchings and A. I. Tartakovskii, *npj 2D Mater Appl*, 2024, **8**, 6.
- 33 S. Liu, A. Granados del Águila, D. Bhowmick, C. K. Gan, T. Thu Ha Do, M. A. Prosnikov, D. Sedmidubský, Z. Sofer, P. C. M. Christianen, P. Sengupta and Q. Xiong, *Phys. Rev. Lett.*, 2021, **127**, 097401.
- 34 J. Cui, E. V. Boström, M. Ozerov, F. Wu, Q. Jiang, J.-H. Chu, C. Li, F. Liu, X. Xu, A. Rubio and Q. Zhang, *Nature Communications*, 2023, **14**, 3396.
- 35 F. Català, F. Marsà, M. Montes-Usategui, A. Farré and E. Martín-Badosa, *Sci Rep*, 2017, **7**, 16052.
- 36 J. Ji, A. Zhang, J. Fan, Y. Li, X. Wang, J. Zhang, E. W. Plummer and Q. Zhang, *Proc. Natl. Acad. Sci. U.S.A.*, 2016, **113**, 2349–2353.
- 37 W. Fu, X. Zhao, K. Wang, Z. Chen, K. Leng, D. Fu, P. Song, H. Wang, L. Deng, S. J. Pennycook, G. Zhang, B. Peng and K. P. Loh, *Nano Lett.*, 2020, **20**, 5330–5338.
- 38 T. Yin, K. A. Ulman, S. Liu, A. Granados Del Águila, Y. Huang, L. Zhang, M. Serra, D. Sedmidubsky, Z. Sofer, S. Y. Quek and Q. Xiong, *Advanced Materials*, 2021, **33**, 2101618.
- 39 Z. Liu, K. Guo, G. Hu, Z. Shi, Y. Li, L. Zhang, H. Chen, L. Zhang, P. Zhou, H. Lu, M.-L. Lin, S. Liu, Y. Cheng, X. L. Liu, J. Xie, L. Bi, P.-H. Tan, L. Deng, C.-W. Qiu and B. Peng, *Sci. Adv.*, 2020, **6**, eabc7628.
- 40 A. Wiedenmann, J. Rossat-Mignod, A. Louisy, R. Brec and J. Rouxel, *Solid State Communications*, 1981, **40**, 1067–1072.
- 41 Q. Xie, S. Hu, C. Hu, Q. Sheng, L. Chen, J. Zheng, W. Wang, L. Ma and G. Cheng, *Applied Physics Letters*, 2023, **122**, 161901.
- 42 D. Jana, P. Kapuscinski, A. Pawbake, A. Papavasileiou, Z. Sofer, I. Breslavetz, M. Orlita, M. Potemski and C. Faugeras, *Phys. Rev. B*, 2023, **108**, 144415.
- 43 Y. Wan, Xing Cheng, Yanfang Li, Lun Dai and Erjun Kan, *RSC Advances*, 2021, **11**, 4035–4041.



Data Availability Statement

The datasets generated and analyzed in this study are available from the corresponding author on reasonable request. All relevant data supporting the findings of this study are included within the article and its supplementary information files.

